Oxidation behavior of Ti_2AlC in the temperature range of 1400°C - 1600°C in steam

Chongchong Tang, Martin Steinbrück, Mirco Große, Thomas Bergfeldt, Hans Jürgen Seifert

Institute for Applied Materials (IAM), Karlsruhe Institute of Technology (KIT), D-76021 Karlsruhe, Germany

Abstract: The oxidation behavior of bulk Ti_2AlC ceramic in steam has been investigated in the temperature range of 1400°C - 1600°C. The oxidation kinetics followed a sub-parabolic law at the early stage of oxidation, then transferred to a linear law beyond 18 hours at 1400°C, and obeyed a linear law during the whole exposure up to 24 hours at 1500°C. At the initial stage of oxidation at 1400°C and 1500°C, randomly Al_2TiO_5 isolated islands with large elongated grains were observed on the surface. A continuous inner α-Al_2O_3 layer with a thin discontinuous outer layer of Al_2TiO_5 formed with prolonged exposure time. Outward diffusion of Ti and C through grain boundaries of the α-Al_2O_3 scale during steady-state oxidation result in segregation of TiO_2 at the grain boundaries of α-Al_2O_3 and formation of gaseous CO and CO_2, respectively. The scale adhesion was reduced in steam compared to that in air due to the accumulation of stresses, and generation of voids at the scale/substrate interface. The mechanical disruption of the oxide scale to relief the stresses contribute to the breakaway oxidation of Ti_2AlC at 1400°C and to the non-protective effect at 1500°C. The sample was rapidly and completely consumed during isothermal oxidation at 1600°C accompanied by release of heat and hydrogen. The maximum tolerant temperature of Ti_2AlC in steam was approximate 1555°C, which can be extended via a tailored pre-oxidation process.

Key words: Ti_2AlC MAX phase; steam oxidation; high temperature; microstructure

1. Introduction

Zirconium alloys have been used in current light water reactors (LWRs) as fuel claddings and other structural materials for several decades due to the low thermal neutron capture cross section, outstanding mechanical performance and reasonable corrosion resistance in hot water [1]. Optimized performances of nowadays nuclear grade zirconium alloys have been achieved within decades of research and operation under normal operation conditions. However, the satisfactory performance of zirconium alloys is challenged when the operating conditions transform from normal to design-basis (DB) or beyond design-basis (BDB) nuclear reactor accident scenarios. The loss of cooling capability inside the core can eventually drive up the fuel temperature and expose the claddings to a high-temperature steam environment for prolonged periods. Once the cladding temperature exceeds around 1000°C, the claddings undergo severe degradation and self-catalyzed oxidation, resulting in large heat release and rapid hydrogen production from exothermic zirconium-steam oxidation [2]. As a result, the cladding, fuel and core structures are at risk of melting, accompanied by hydrogen explosion and associated release of highly-radioactive fission products, such as the accident in the Fukushima Daiichi nuclear power plants [3]. Hence, the inherent weaknesses of this uranium dioxide-zirconium alloy system under severe accident conditions promotes the shift of researching focus from improving nuclear fuel performance to advanced fuels under DB and BDB condition and the establishment of accident-tolerant fuels (ATFs) concept post-Fukushima [4,5]. The novel ATF claddings should tolerate temperature much higher than 1200°C for a significantly longer time, along with improved performance under normal operating conditions.

Different categories of materials, like stainless steels, ODS alloys, SiC and $M_{n+1}AX_n$ phases, are being investigated to possibly replace zircaloy used in current light water reactors [5,6]. The $M_{n+1}AX_n$ (MAX) phases, where M is an early transition metal, A is a group 13 - 16 element and X

is C and/or N, represent a family of layered ternary carbides and nitrides, which have attracted a great deal of attention in recent decades due to their unique combination of metallic and ceramic properties [7]. Similar to metals, they are readily machinable, possess good thermal and electrical conductivities, excellent damage tolerance and thermal shock resistance. Meanwhile, they are lightweight, relatively soft, elastically stiff, and resistant to oxidation and corrosion like their binary carbide and nitride counterparts [8]. Due to their good properties, MAX phases have been considered as both cladding materials and protective coatings for current light water reactors and future nuclear industry [9,10]. Recent work has shown that some MAX phases, especially Ti_3SiC_2 and Ti_2AlC, are resistant to both heavy ion irradiation and neutron irradiation, maintaining phase stability and crystallinity up to high displacement per atom (dpa) [11–13]. The interactions between Zircaloy-4 and these two MAX phases in the 1100°C - 1300°C range has also been investigated recently [9].

The high-temperature oxidation behaviors of Ti_3SiC_2 and Ti_2AlC have been extensively investigated. The high-temperature oxidation of Ti_3SiC_2, in all cases, results in the formation of a duplex scale: an outer rutile layer and an inner rutile/silica mixed layer. The oxidation kinetics becomes linear at temperature higher than 1000°C after exposure times greater than 30 h in air [14,15]. Therefore, the failure establishment of protective scale on the surface of Ti_3SiC_2 during high-temperature oxidation will certainly limit its application as high-temperature material. Furthermore, Al-containing MAX phase (Ti_3AlC_2) also demonstrates better hydrothermal oxidation resistance than Ti_3SiC_2 due to the higher stability of alumina than silica in hydrothermal water [16]. It has been confirmed that Ti_2AlC shows both excellent high-temperature isothermal and cyclic oxidation resistance whether in air or in humid atmosphere [17–22]. The selective oxidation of aluminum and the small difference in the coefficients of thermal expansion (CTE) between Al_2O_3 and Ti_2AlC substrate contribute to the formation of a slow-growing, adherent and dense α-Al_2O_3 layer on the surface of Ti_2AlC during high-temperature oxidation. Two different kinetics, parabolic law or cubic law, have been proposed to describe the oxidation of Ti_2AlC in

the temperature range of 1000°C - 1400°C when exposed to air or steam. One critical review by Tallman et al. [22] well explained that the oxidation kinetics in air was better described by cubic kinetics due to the grain coarsening effect at the oxide/substrate interface. Prior to this cubic steady-state oxidation kinetics, significant transient oxidation during the initial stage of oxidation due to the rapid growth of non-protective TiO_2 scale was demonstrated [21]. Moreover, autonomous high-temperature crack-healing behavior has been reported for Ti_2AlC due to a relatively high diffusivity of the Al and a sufficient volume expansion during oxidation [23,24]. Few studies have extended the oxidation temperature to 1400°C in air [25,26], but no reports are found on the oxidation of Ti_2AlC up to 1400°C in steam. Under BDB nuclear reactor accident scenarios, the cladding can be exposed to an extremely high-temperature steam environment, like higher than 1500°C, for prolonged periods [3]. Before considering the application for current light water reactors, however, it is crucial to understand its oxidation behavior in the high-temperature steam environment.

The purpose of this study is to determine the oxidation behavior of bulk Ti_2AlC ceramic at the 1400°C - 1600°C range and its maximum temperature capability in steam. The experiments were all conducted in a tube furnace under well-defined atmospheres, coupled with a mass spectrometer to monitor the composition of the released gases, especially of hydrogen and carbon oxides. The oxidation mechanism and failure mechanism in high-temperature steam are discussed based on the oxidation kinetics and microstructure evolution of the scales formed on the surface of Ti_2AlC samples.

2. Experimental details

2.1 Samples

A dense Ti_2AlC bulk plate of Maxthal® 211 (Ti : Al : C=2.0 : 1.02 : 0.99, mol) was purchased from Kanthal/Sandvik, Sweden. The measured density is around 3.99 g/cm^3 (99% theoretical). Rectangular specimens for oxidation experiments with a dimension of approximately 3 × 6 × 10 mm^3 were cut by conventional band saw. The surfaces were ground to 2400 grit with SiC paper, then washed in ultrasonic solution with the sequence of 10 min deionized water, 10 min acetone, 10 min isopropanol, finally dried in hot air. The specimens are predominantly composed of Ti_2AlC MAX phase with a small quantity of Ti_3AlC_2 MAX phase identified by XRD. The free carbon in the specimens was analyzed according to Standard ASTM C791 (3M Technical Ceramics, Germany). The specimen was cut and ground into powder. The free carbon was analyzed by wet-chemical oxidation with iodine/chromic acid at 85°C and 120°C in a CS-analyzer from behr (CS 30 HT). The results demonstrated that the specimens contained around 2.39 wt.% free carbon by measuring the released CO_2.

2.2 Experimental setup

All the oxidation experiments in this study were conducted in a horizontal corundum tube furnace (Φ: 40 mm) under normal pressure. The specimen stood on a corundum sample holder with narrow face down and was placed at the center of the furnace. The furnace temperature was controlled by a mantled thermocouple located in the upper part of the furnace tube near the sample. The specimens were isothermally oxidized in a flowing argon + steam atmosphere. The gas atmospheres were controlled by Bronkhorst® flow controllers and a Bronkhorst® CEM System (Controlled Evaporation and Mixing), meanwhile, the composition of the off-gas was *in-situ* analyzed by a mass spectrometer Balzers GAM300 with accuracy up to 1 ppm. The flow rates of each gas are given in standard conditions (25°C, 1bar). All the specimens, except one ramp test and two comparison isothermal oxidation tests in air, were heated in high purity Ar

atmosphere (99.9999%) to the desired temperature with a gas flow rate of 40 l/h Ar, then the atmosphere was changed to 20 l/h Ar and 20 g/h H_2O for steam oxidation test with different dwell time. Argon was used as the carrier gas and also the reference gas for mass spectrometer analysis. The steam flow rate was selected at this level based on the instrument configurations as well as to ensure no steam starvation during oxidation process. Finally, the specimens were cooled down to room temperature also in high purity Ar atmosphere with a gas flow rate of 40 l/h Ar in the furnace. The heating and cooling rates were kept at 10 K/min. The concentration of H_2O during isothermal oxidation was ~55 vol%. Fig.1 illustrates the typical heating and gas flow rate history of an isothermal oxidation test. Isothermal oxidation tests at 1400°C and 1500°C with six different time periods from 1 hour to 24 hours and at 1600°C with one time (6 hours) were conducted. The ramp oxidation test from 500°C to 1600°C was conducted to determine the maximum tolerant temperature of Ti_2AlC via the oxidation kinetics reflected by the hydrogen release rate. The two comparison isothermal oxidation tests in air were performed at 1400°C for 24 hours and at 1500°C for 12 hours with the same settings except that the steam was replaced by 20 l/h air during isothermal period.

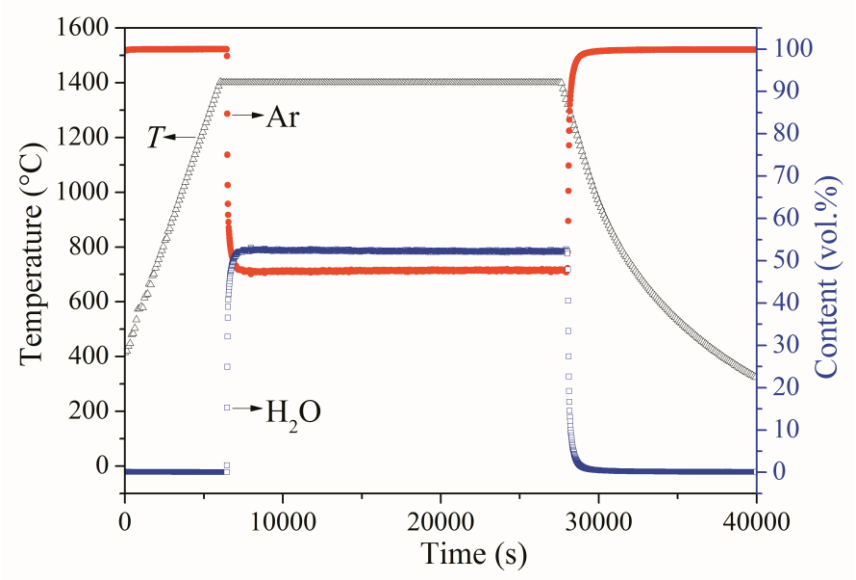

Fig.1 Typical heating and gas flow rate history during isothermal oxidation test in steam.

2.3 Post-test examinations

The mass of the samples were measured using an analytical balance with a resolution of 0.0001 g before and after oxidation. The phase compositions of the oxide scale on the oxidized samples were characterized using X-ray diffraction (XRD, Seifert PAD II) with Cu $K_{\alpha 1}$ radiation (λ=0.154 nm, 40 kV and 30 mA) in Bragg–Brentano geometry (θ-2θ) with a step size of 0.002 ° and a scan speed at 1 °/min. The surface and cross section microstructures were determined using a field-emission scanning electron microscope (SEM, Philips XL30S), equipped with energy dispersive X-Ray spectroscopy (EDS) for element analysis. For cross-sectional metallographic examination, the oxidized samples were mounted with epoxy resin. After sufficient hardening of the epoxy, the samples were firstly ground using resin bonded diamond grinding discs starting from 220 down to 1200, then polished with a sequence of 15, 6 and 3 μm diamond paste and finally rinsed with active oxide polishing suspensions and water. Then the polished samples were cleaned in an ultrasonic bath followed by deionized water and acetone. A thin layer of gold was deposited on the surfaces and cross sections of the oxidized samples before SEM observation.

3. Results

3.1. Isothermal oxidation at 1400°C and 1500°C in steam

3.1.1. Oxidation kinetics

The oxidation kinetics, i.e. mass change per unit area as a function of time, of the Ti_2AlC samples oxidized at 1400°C and 1500°C up to 24 hours in steam are shown in Fig.2 (a); the mass change after oxidation in air were also inserted in the figure. Fig.2 (b) shows the post-test surface appearances of the samples after three different time periods 1, 12 and 24 hours, respectively. As can be seen from Fig.2 (a), the mass gain increased slowly with prolonged exposure time up to 12 hours at 1400°C in steam. A slight deviation of the mass gain, i.e. faster oxidation rate, was observed when the exposure time exceeded 18 hours. At 1500°C, the rise of mass gain was

significantly faster than that at 1400°C. Weight loss emerged due to significant spallation of the oxide scale when the exposure time reached 18 hours.

The typical power law of the oxidation kinetics can be written as:

$$\Delta W/A = K t^n \quad (1)$$

where $\Delta W/A$ is the mass change per unit surface area, K is the rate constant, t is oxidation time, and n is the time exponent. Several representative oxidation kinetics correspond to different time exponents, 1 for linear, 1/2 for parabolic, 1/3 for cubic and 1/3-1/2 for sub-parabolic [27]. After evaluation of the weight change vs. oxidation time data, sub-parabolic law and linear law were adopted to describe the oxidation kinetics at the early stage of oxidation at 1400°C and 1500°C in this study, respectively. The solid curves in Fig.2 (a) show the fitting results ignoring the last two points in each series. At 1400°C up to 12 hours, the time exponent of the sub-parabolic law was calculated as 0.399, nearly cubic (1/3) oxidation kinetics. The oxidation kinetics transformed from sub-parabolic law to linear law, i.e. breakaway oxidation, after prolonged exposure at 1400°C. This transformation is proved by the *in-situ* measured hydrogen production rate which will show later. At 1500°C, the oxidation kinetics maintained a linear law from the initial stage of oxidation. The different growth kinetics combined with high values of correlation coefficients (shown in Fig.2 (a)) reflected different growth rate-limiting steps at 1400°C and 1500°C. As shown in Fig.2 (b), for the Ti_2AlC samples oxidized at 1400°C the oxide scales formed on the surface remained adherent, showing compact structure after 12 hours oxidation. Partial delamination of the scale was observed, especially along the edges of the sample, after oxidation for 24 hours. However, the scale did not spalled off and the mass gain was only 3.24 mg/cm^2 after exposure in steam for 24 hours at 1400°C. Apparently, transformation of the surface appearances after oxidation at two different temperatures was observed, black at 1400°C to gray at 1500°C. At 1500°C, the scale structure was relatively loose even after short time oxidation and large areas of the scale spalled off after oxidation for 24 hours. It demonstrated that the oxide scale formed on the surface of Ti_2AlC substrate lost protection at 1400°C after prolonged

exposure and at 1500°C from the beginning of oxidation. Therefore, the mechanical disruption observed, like delamination and porous structure, of the scales provide short-circuit diffusion paths for the oxidizing gas, accounting for the different oxidation kinetics. The evolution of the surface appearances are in accordance with the change of mass gains versus oxidation time. Compared to the samples oxidized in steam, oxidation of the samples in air at 1400°C for 24 hours and at 1500°C for 12 hours resulted in slightly lower mass gain. In terms of surface appearances, there was no partial delamination observed at 1400°C for 24 hours and more dense scale structure showed at 1500°C for 12 hours in air compared to those in steam (not shown here, see SEM images of discussion section).

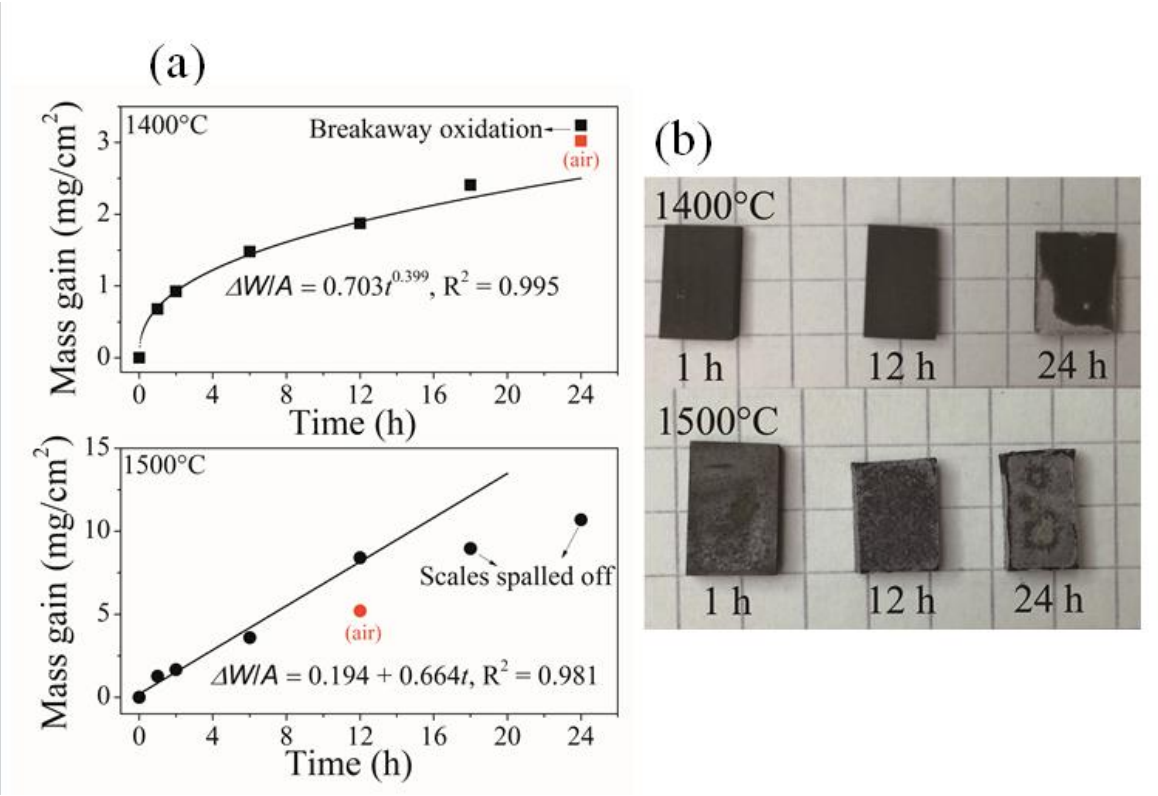

Fig.2 Oxidation kinetics and surface appearances of Ti_2AlC after oxidation at 1400°C and 1500°C in steam. (a) Mass gain per unit surface area as a function of time with two tests in air. The solid curves indicate fitting relationship between mass gain and oxidation time up to 12 hours. (b) Post-test surface appearances at three different time periods: 1, 12 and 24 hours. The grid in the picture is 5 mm.

3.1.2 Gas release during oxidation

Eight different gaseous species, including H_2, CH_4, H_2O, N_2, CO, CO_2, O_2 and Ar, in the off-gas were analyzed on-line using a mass spectrometer. Fig.3 shows the representative flow rates of three concerning gases (H_2, CO, CO_2) as a function of time for the Ti_2AlC samples oxidized at 1400°C (Fig.3 (a)) and at 1500°C (Fig.3 (b)) for 18 hours in steam (similar flow rate behavior was observed for other tests). The time interval is selected ignoring the initial oxidation period of steam inlet. At the early stage of oxidation, a similar tendency was observed for H_2 release rates both at 1400°C and 1500°C, i.e. the flows increased slowly to reach a plateau. In addition, the rising period of the hydrogen release rate increased with the rising of oxidation temperature, around 1 hour at 1400°C grown to 2 hours at 1500°C (dotted lines in Fig.3). After this rising period, the hydrogen flow decreased gradually at 1400°C and remained somehow constant at 1500°C. The increasing hydrogen release rate during the initial period of oxidation at 1400°C demonstrated faster oxidation rate at the early stage of oxidation than that at the steady-state oxidation, which can be attributed to the transient oxidation with rapid growth of titanium dioxide and will be discussed later. The H_2 release rates after the rising period could be described by a negative exponent law at 1400°C for certain oxidation time up to around 12 hours and a linear law at 1500°C, and then tended to be linear at 1400°C for longer time exposure as shown by the fitting lines. Consistent with the mass change data shown in the previous part, these observations indicated that the oxidation kinetics firstly followed a sub-parabolic law, then transformed to a linear law at 1400°C and maintained a linear law at 1500°C. The flow rate of hydrogen during the steady-state oxidation at 1500°C (around 0.04 $l \cdot cm^{-3} \cdot h^{-1}$) is one magnitude higher than that at 1400°C (around 0.005 $l \cdot cm^{-3} \cdot h^{-1}$), demonstrating much faster oxidation rate at 1500°C than at 1400°C, in accordance with the mass gain tendency before.

As shown in Fig.3, both CO and CO_2 gas flow were detected once Ti_2AlC samples were exposed to steam after eliminating the impact of atmosphere change. The flow rate of CO_2 is higher than that of CO. Hence, a small quantity of C in Ti_2AlC or free carbon in the specimens

was oxidized to form gaseous CO_2 and/or CO, mainly CO_2, during the oxidation process. A slight increase of the flow rate of CO_2 was observed with prolonged exposure at both temperatures as shown with the dashed lines or the images were enlarged.

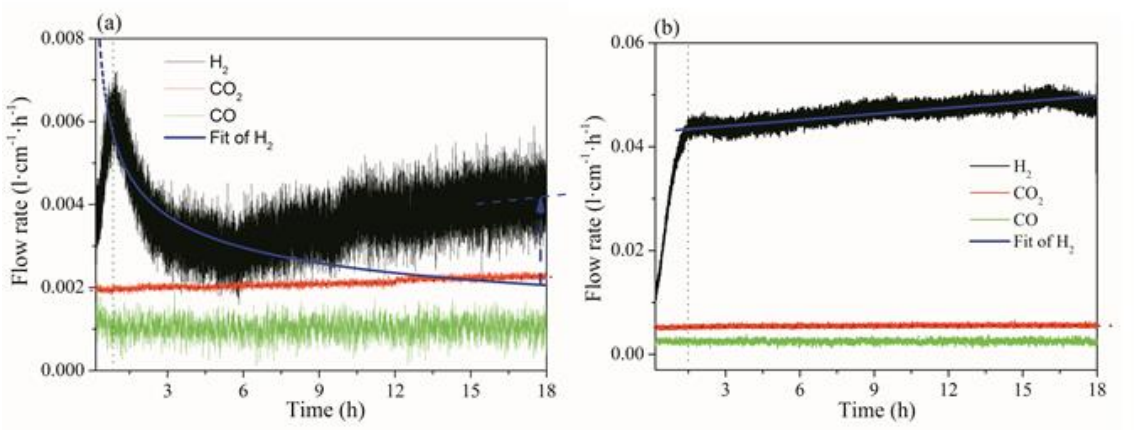

Fig.3 Flow rates of H_2, CO, CO_2 per surface area as a function of time for the Ti_2AlC samples oxidized in steam at (a) 1400°C and (b) 1500°C for 18 hours.

3.1.3 Phase evolution of the oxide scale

The evolution of phase compositions that formed on the surface of the Ti_2AlC samples after oxidation at 1400°C and 1500°C for six different time periods in steam was identified by XRD, and the results are shown in Fig.4. Only three distinct phases were detected, i.e. Ti_2AlC (PDF card No. 29-0095), α-Al_2O_3 (PDF card No. 43-1484) and Al_2TiO_5 (PDF card No. 41-0285), for all the samples after oxidation. The relatively high intensity of diffraction from Ti_2AlC substrate even after oxidation at 1400°C for 24 hours revealed low thickness of the α-Al_2O_3 scale formed on the surface of Ti_2AlC substrate. The intensity of diffraction associated with α-Al_2O_3 increased significantly at 1400°C and fluctuated at 1500°C with increasing oxidation time. The absence of the TiO_2 phase and the appearance of the Al_2TiO_5 phase indicated the reaction between TiO_2 and Al_2O_3 to form Al_2TiO_5. The phase diagram of the TiO_2 - Al_2O_3 system confirms that this reaction occurs at around 1200°C [28] and Al_2TiO_5 phase was also observed by previous studies for Ti_2AlC oxidation above 1200°C [18,26]. It is necessary to notice that the signal intensity of Al_2TiO_5 phase was significantly lower compared to those of Ti_2AlC and α-Al_2O_3 at both

temperatures, suggesting that the content of Al_2TiO_5 was negligible and the predominant phase in the oxide scale was α-Al_2O_3.

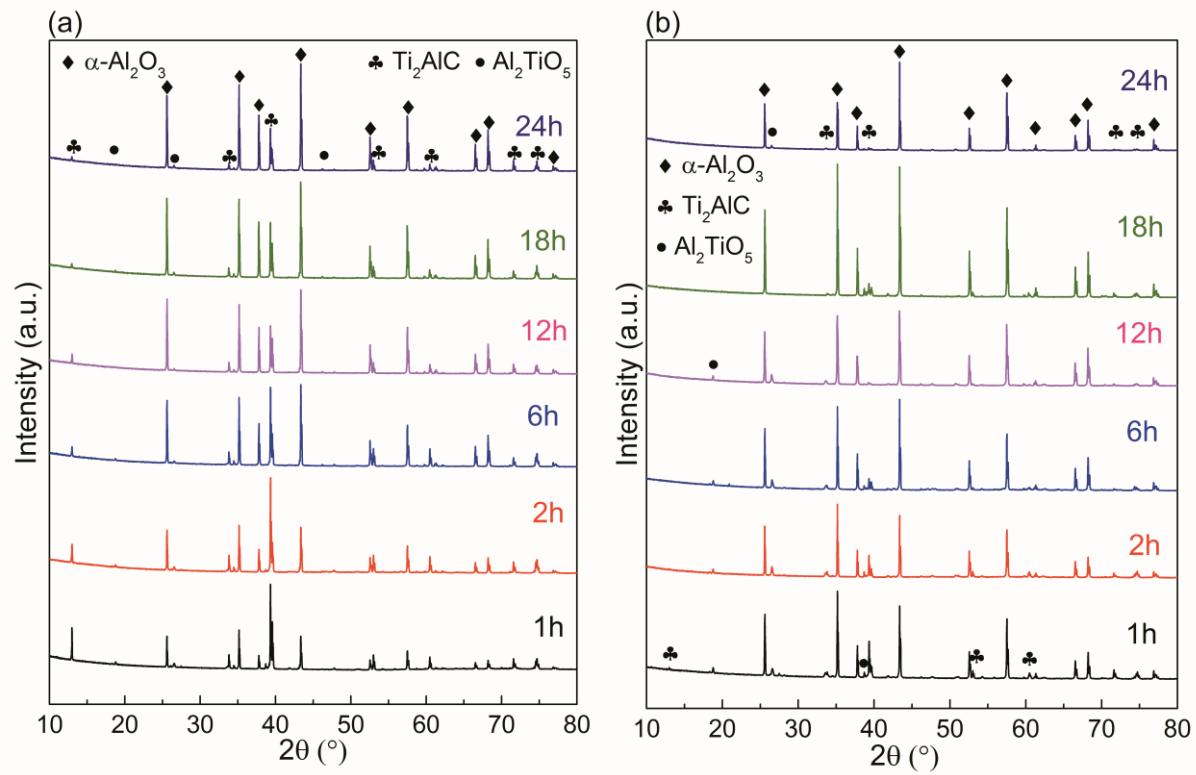

Fig.4 X-ray diffraction patterns of oxide scales formed on the surface of Ti_2AlC at (a) 1400°C and (b) 1500°C in steam for six different time periods.

3.1.4 Morphology evolution of the oxide scale

Fig.5 shows the SEM images of typical surface morphologies of Ti_2AlC oxidation at 1400°C and 1500°C in steam after different time periods with corresponding EDS measurements. After exposure at 1400°C in steam for 1 hour, as shown in Fig.5 (a), the surface of Ti_2AlC was rough, consisted of randomly isolated islands with large elongated grains embedded in a coarse appearance with small irregular grains. EDS elemental analysis (Fig.5 (g)) demonstrated that the isolated islands were Ti-enriched, and the stoichiometry was close to Al_2TiO_5 identified by XRD (point 1). These islands cracked and contained micro-cracks. The remaining surface was covered by alumina scale (point 2) with dense and columnar grain structure. The density and size of the

isolated islands decreased with prolonged exposure time at 1400°C. When the oxidation time reached 12 hours at 1400°C, as shown in Fig.5 (b) with EDS line-scanning profiles, these Ti-enriched islands disappeared and the surface became coarser and consisted of a discontinuous Ti-enriched outer layer. It was necessary to note that same isolated islands were also observed after oxidation at 1500°C for 1 hour, as shown in Fig.5 (d), except that the dimension was much smaller by an order of magnitude. The scale remained adherent and crack-free at 1400°C for 1 and 12 hours, however, micro-cracks were observed at 1500°C on oxidized samples for 1 hour as shown in Fig.5 (a) and (d), respectively. Partial detachment of the scale, especially along the edges, was observed on the sample oxidized at 1400°C for 24 hours as shown in Fig.5 (c), whereas, the detached scale became considerably loose and porous compared to the undetached areas. A similar loose structure of the oxide scale throughout the surface was obtained after oxidation at 1500°C for 12 hours as shown in Fig.5 (e). These observations explain the different oxidation kinetics obtained at 1400°C and 1500°C. After oxidation at 1500°C for 24 hours in steam, the scale showed significant spallation and cracks.

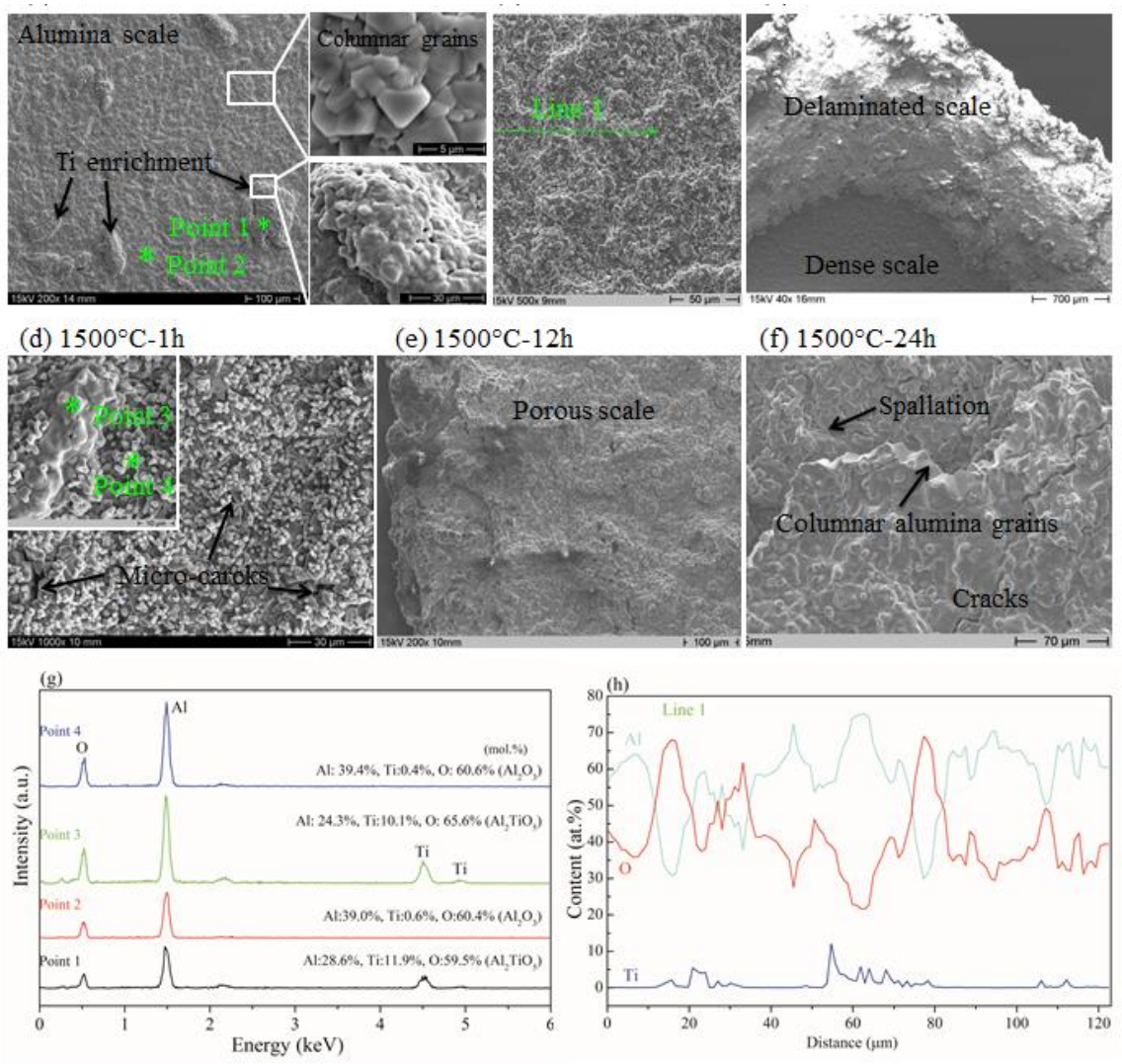

Fig.5 SEM images of typical surface morphologies of Ti_2AlC after oxidation at 1400°C and 1500°C in steam with different time periods and corresponding EDS measurements. See text for detailed description.

To further understand the oxidation behavior of Ti_2AlC at 1400°C and 1500°C in steam, the cross-section morphologies after three different oxidation time periods were also examined by SEM. The results are shown in Fig.6 including two representative EDS line-scanning profiles. Clearly, the alumina oxide scale maintained adherent, dense and grew slowly at the early stage of oxidation at 1400°C in steam. The thickness of the oxide scale grew from around 3.5 μm for 1 hour (Fig.6 (a)), to nearly 10 μm for 12 hours (Fig.6 (b)). The inserted BSE image in Fig.6 (a) identified the external Al_2TiO_5 isolated islands above the α-Al_2O_3 scale at the early stage of oxidation. Micro-cracks were observed within the islands, but the beneath scale was crack-free.

For samples oxidized 24 hours at 1400°C in steam, the oxide scale delaminated and became loose as shown in Fig.6 (c), indicating that the oxide scale lost protective effect at prolonged exposure time and in agreement with the transformation of oxidation kinetics from sub-parabolic law to linear law over oxidation time. A ragged appearance was observed for the sample oxidized at 1500°C in steam for just 1 hour (Fig.6 (d)). The scale was relatively dense; the micro-cracks observed on the surface (Fig.5 (d)) seems have not penetrated through the alumina scale. The structure of oxide scales became loose with increasing exposure time (Fig.6 (e) and (f)). Two oxide layers separated by resin and fracture of the upper oxide scale were observed. The structure of the α-Al_2O_3 grain was confirmed as columnar.

Fig.6 (g) and (h) illustrate the content profiles of O Al and Ti by EDS along the green lines shown in Fig.6 (b) and (f) of samples oxidized at 1400°C for 12 hours and at 1500°C for 24 hours in steam, respectively. Several distinctive zones were observed across the oxide scale/ambient interface to substrate/oxide scale interface and displayed as different numbers. Beneath zone 1, which is resin used to embed samples, a thin Ti rich layer (zone 2) is presented on the external surface of the oxide scale in both profiles. The mole ratio of Al and O concentrations was approximate 2:3 in the oxide scales of zone 3 in Fig.6 (g) and zone 7 in Fig.6 (h), indicating growth of α-Al_2O_3 throughout the oxide scale. It is important to note that a similar Ti-enriched layer (zone 6) was also observed on the external surface of the undetached oxide scale in Fig.6 (h), even the peak intensity was weak. Another interesting finding is that peaks of Ti element present at the grain boundary of alumina grains as shown zone 4 in Fig.6 (h), indicating outward diffusion of Ti during the oxidation process, then oxidized and reacted with α-Al_2O_3 to form Al_2TiO_5 as discussed in the XRD part. Meanwhile, titanium oxides segregated at the grain boundaries of α-Al_2O_3 grains.

A thin Al-depleted and Ti-rich layer, around 1 μm thick, was observed beneath the Al_2O_3 scales, as shown in Fig.6 (g) zone 4 of Ti_2AlC oxidation at 1400°C for 12 h. Such Al-depleted layer has not been observed in previous studies at lower oxidation temperature except by using

TEM [29,30]. The appearance of this Ti-rich layer observed by SEM-EDS in our study probably attributes to enhanced diffusion rates of Al and faster growth of Al_2O_3 scale during high-temperature oxidation in steam. However, this layer was somehow inconspicuous for Ti_2AlC oxidation at 1500°C for 24 h as shown in Fig.6 (h) zone 8. The reason is probably because the loose structure of oxide scale at 1500°C can considerably increase the outward diffusion rate of Ti and C during oxidation as shown in Fig.3.

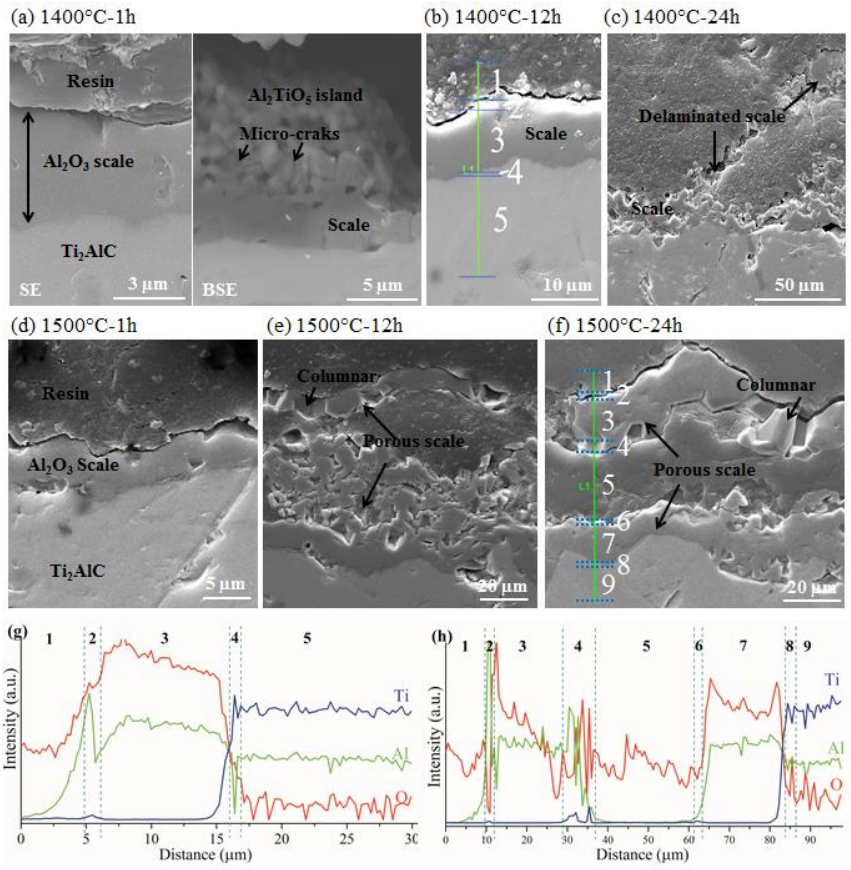

Fig.6 SEM images of typical cross section morphologies of Ti_2AlC oxidation at 1400°C and 1500°C in steam with different time periods and the line-scanning profiles along the green line top down in (b) and (f). See text for detailed description.

3.2 Oxidation at 1600°C in steam

While the forming scale on the surface of Ti_2AlC lost its protective effect at 1500°C in steam, it is essential to define its highest temperature capability to figure out gains in safety margins for application as a new potential cladding material. Two different tests, i.e. one isothermal test and one ramp test starting from 500°C with heating rate 10 K/min, up to 1600°C were conducted. Fig.7 and Fig.8 show the flow rates of several off-gases and XRD patterns of the surface for the Ti_2AlC samples oxidized at 1600°C in the isothermal test and the ramp test, respectively.

As can be seen from Fig.7 (a), the flow rates of H_2 and CO_2 in the off-gas were driven up to extremely high levels compared to that oxidation at 1400°C (more than one hundred times higher), and then decreased quickly. After examination of the morphology and mass change of the sample (around 35 wt.% mass gain), it was believed that the sample was quickly and completely consumed. The XRD result (Fig.8) showed that the phase compositions of the surface contained only two phases after the isothermal test, TiO_2 and Al_2TiO_5, indicating that Ti_2AlC failed to form a protective oxide scale at 1600°C in steam. The overall reaction of Ti_2AlC and steam at 1600°C can be written as

$$Ti_2AlC + 15/2H_2O = 3/2TiO_2 + 1/2Al_2TiO_5 + CO_2 + 15/2H_2 \quad (2)$$

The standard enthalpy of formation and heat capacity of Ti_2AlC were reported previously [31,32]. The enthalpy of this reaction at 1600°C is calculated to be around -940 kJ/mol, and slightly lower at 1500°C and 1400°C. This demonstrates that a large amount of hydrogen and heat will be released once Ti_2AlC is exposed to severe oxidation in high-temperature steam.

Fig.7 (b) shows the flow rates of several gas species during the ramp test up to 1600°C. The flow rates of all gases, except for H_2, remained small and nearly constant. The release rate of H_2 increased gradually up to around 1555°C, then accelerated and the slope of the curve became much pronounced. Hence, severe oxidation of Ti_2AlC may occur at about 1555°C in steam without pre-oxidation. However, in the ramp test the flow rate of H_2 at 1600°C was several times

lower than that in the isothermal test, and the XRD result (Fig.8) indicated that an α-Al_2O_3 scale formed on the surface of the sample, which protected the sample from fast consumption. Therefore, it can be predicted that the maximum tolerant temperature of Ti_2AlC in steam can be extended via a tailored pre-oxidation process.

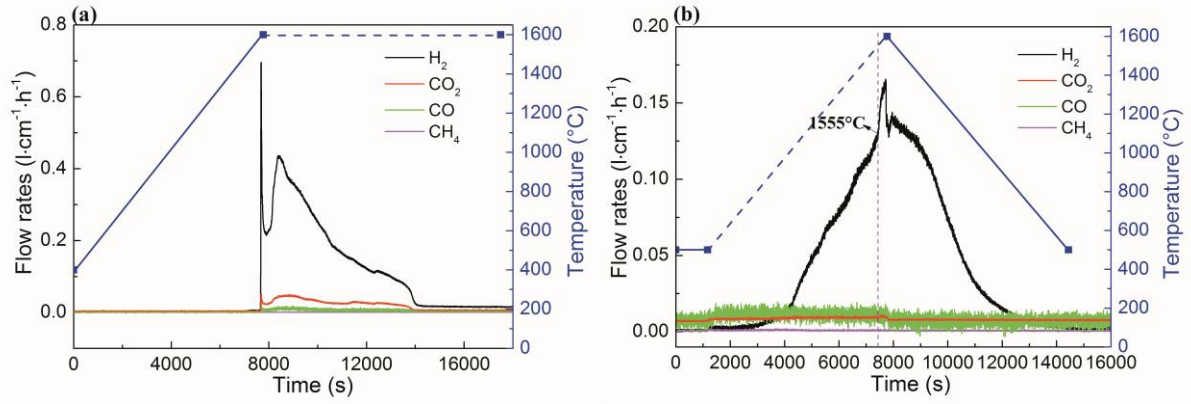

Fig.7 Flow rates of H_2, CO_2, CO, and CH_4 in the off-gas as a function of time for the Ti_2AlC samples oxidized at 1600°C (a) isothermal test and (b) ramp test. The blue solid line and blue dashed line of the temperature signal represent conditions of pure argon and of a mixture of steam and argon, respectively.

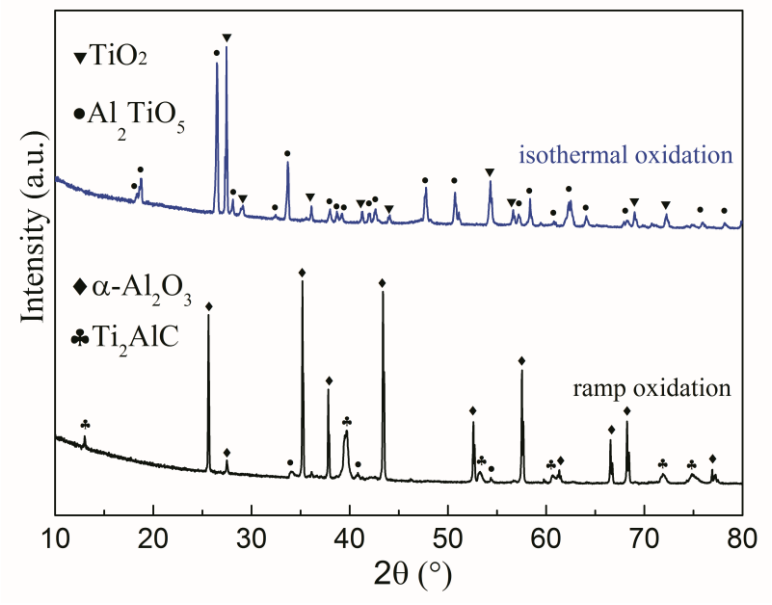

Fig.8 X-ray diffraction patterns of the surface of Ti_2AlC oxidized at 1600°C in steam for the isothermal test (top) and the ramp test (bottom).

4. Discussion

4.1 Oxidation mechanism

It is generally believed that water vapor has little effect on the oxidation kinetics of alumina-forming materials except the scale adhesion is reduced [17,20,33]. Fig.9 shows the SEM images of typical surface morphologies of Ti_2AlC after oxidation at 1400°C for 24 h and 1500°C for 12 h in air. This conclusion is confirmed in this study for the oxidation of Ti_2AlC by comparing the oxidation results in steam and in air. Compared to the sample surfaces after oxidation at same temperature and time in steam (Fig.5), the alumina scales here are denser and show better adherence. No delamination or spallation was observed even around the edges. A transient oxidation stage emerges before the establishment of protective alumina scale due to the competitive and selective oxidation of Al and Ti atoms in the Ti_2AlC matrix with the change of oxidant partial pressure at the oxide/substrate interface [17,21]. Upon exposing the Ti_2AlC sample to elevated temperature steam, a thin oxide layer corresponding to the initial surface which contains a high concentration of base elements, in this case Ti and Al, is supposed to firstly develop on the surface of the samples. The structure of this layer is usually loose and contains structural defects, like pores and cracks, depending on the surface conditions, volume changes and CTEs mismatch of matrix and forming oxides [21,34]. Hence, the steam partial pressure at the oxide scale/substrate interface is high enough to promote both oxidation of Ti and Al. Further oxidation leads to the fast diffusion of Ti through this layer and rapid growth of TiO_2 grains at the oxide scale/ambient interface, leaving randomly Ti-enriched (Al_2TiO_5) isolated islands on the surface during the initial stage of oxidation as observed in Fig.5 (a), (d) and Fig.6 (a). Simultaneously, alumina starts to nucleate at the oxide scale/substrate interface due to alumina represents the most stable oxide in this system. At temperatures higher than 1200°C, TiO_2 and Al_2O_3 react to form Al_2TiO_5.

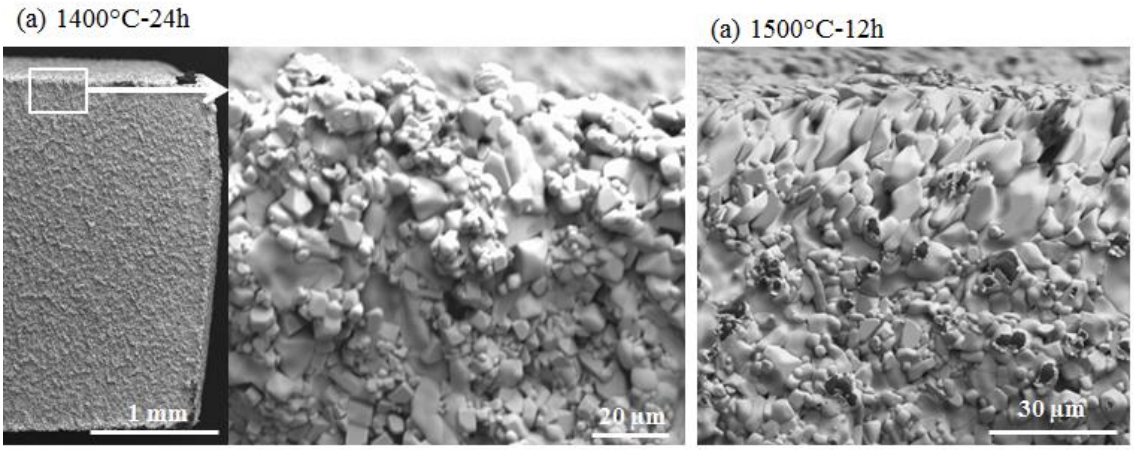

Fig.9 SEM images of typical surface morphologies of Ti_2AlC after oxidation at (a) 1400°C for 24 h and (b) 1500°C for 12 h in air.

At 1400°C and 1500°C, after this transient oxidation stage the inward diffusion of oxidant and outward diffusion of Al becomes the rate determining step which prompts the selective oxidation of aluminum and thickening and roughing of this protective α-Al_2O_3 scale as shown in Fig.6. Fast outward diffusion of Ti and growth of Al_2TiO_5 on the surface is suppressed, however, outward diffusion of Ti ions through α-Al_2O_3 grain boundaries during steady state oxidation continues as exhibited in Fig.6 (h) zone 4, causing segregation of titanium oxide at alumina grain boundaries [29,30]. The oxidation resistance of Ti_2AlC has been compared with some conventional Al_2O_3-forming materials, especially FeCrAl alloys. One obvious advantage of Ti_2AlC is the good CTEs match of Ti_2AlC ($8.5 – 9.6\times 10^{-6}$ K^{-1}) [35,36] substrate and α-Al_2O_3 (8.5×10^{-6} K^{-1}) [26] scale resulting in superior spallation resistance of growth oxide scales. Reactive elements (REs), like Zr, Y, Ti, are introduced into the FeCrAl alloys due to their profound effect on improving the oxidation resistance. Their oxides segregate at the Al_2O_3 grain boundaries to reduce the outward transport of Al, moreover, alter the oxide grain structure from equiaxed to columnar [37,38]. The segregation of TiO_2 at the Al_2O_3 grain boundaries [29] and the transformation of oxide grains from equiaxed to columnar [22] during Ti_2AlC oxidation also have been demonstrated by previous studies and are further confirmed in this study (Fig.6 and 7). Hence, it is reasonable to suggest that Ti in the Ti_2AlC matrix can act as a "reactive element" and TiO_2 segregates at the

Al_2O_3 grain boundaries during high-temperature oxidation. Good CTEs match between Ti_2AlC and α-Al_2O_3 in combination with segregation of TiO_2 in α-Al_2O_3 grain boundaries contribute to the slow growth rate, i.e. nearly cubic kinetics, of α-Al_2O_3 scale forming on the surface of Ti_2AlC oxidation at 1400°C in steam.

The generation of gaseous Ti-containing species, especially $TiO(OH)_2$ through the following reaction

$$TiO_2(s) + H_2O(g) = TiO(OH)_2(g) \quad (3)$$

was confirmed for Ti_2AlC oxidation in steam above 1200°C [17] and hot-pressed Ti-containing compositions in high-temperature steam [39]. The reduction of the dimensions at higher temperature and eventually disappearance of the Ti-enriched isolated islands with prolonged exposure time as shown in Fig.5 may be explained by the generation of gaseous Ti-containing species. The formation of volatile Ti-containing gaseous in steam is supposed to become more pronounced with higher oxidation temperature, which can be seen from the XRD results and morphologies of the samples displayed before. Cui et al. [19] proposed that large CTEs mismatch of Al_2O_3 - Al_2TiO_5, the CTEs anisotropy in Al_2TiO_5 grains, and the large volume changes associated with the reaction of forming Al_2TiO_5 during Ti_2AlC oxidation in air triggered micro-cracks which propagated into the α-Al_2O_3 layer at 1400°C once the Al_2TiO_5 grains exceed the critical size. Same micro-cracks were observed within the Al_2TiO_5 isolated island in this study (Fig.6 (a)), but the α-Al_2O_3 layer beneath remained dense without formation of micro-cracks. Therefore, it is reasonable to believe that the inhibited grain growth of Al_2TiO_5 due to the volatilization of TiO_2 prevents the propagation of micro-cracks into the α-Al_2O_3 scale.

Even though extensive studies have been done to investigate the oxidation behavior of Ti_2AlC, the exact nature of carbon oxidation from Ti_2AlC is poorly understood. Wang and Zhou [18,40] proposed that carbon oxide formed at the oxide/substrate interface, then diffused through the grain boundaries in the oxide layer. Tallman et al. [22] supposed that carbon diffused through the

Al_2O_3 scale and was oxidized to carbon dioxide on the surface. Assuming the carbon was oxidized by inward diffusion of oxidant gas, the flow rates of carbon oxides were predicted to decrease gradually after the transient oxidation stage like the flow rate of hydrogen for the Ti_2AlC oxidation at 1400°C due to decreasing oxidation rate. However, the flow rate of CO_2 slowly increased with prolonged exposure time as shown in Fig.3 (a). The structure of M_2AX phases consists of M octahedral cages with the X atoms filling the octahedral sites and interleaved layers of pure group-A element, resulting in relatively weak bonding of Ti - Al and stronger bonding of Ti - C with high migration rate of aluminum in Ti_2AlC [41]. During high-temperature oxidation, the outward diffusion of Al to form alumina scale usually leaves a thin Ti-rich and Al-depleted intermediate layer between the oxide scale and the substrate [30,42]. As shown in Fig.6, a thin Ti-rich layer was also observed in this study between the α-Al_2O_3 scale and Ti_2AlC substrate. Hence, this layer or the free carbon in the matrix could act as C reservoir. Besides, the diffusion of carbon from Ti_2AlC thin films into single crystal α-Al_2O_3 substrate above 570°C has been confirmed [43]. Based on above observations, it is reasonable to suggest that a small quantity of C diffuses through the Al_2O_3 scale to the surface, and is subsequently oxidized to form CO_2 and/or CO, mainly CO_2 determined by mass spectrometer.

4.2 Failure mechanism

In this study, slightly faster oxidation rate was obtained for Ti_2AlC oxidation at 1400°C and 1500°C in steam compared to that in air. Similar observation can be obtained compared with previous studies [17,26]. One critical review [44] on different species diffusion in alumina demonstrated that the diffusion coefficient of water is higher than that of oxygen both in single crystal and poly-crystalline alumina with much lower activation energies. The easy diffusion of water attributes to different types of hydrogen-containing species [33], especially hydroxide ions, generated by the following equilibrium reaction,

$$H_2O + O_O^X + V_O^{\cdot\cdot} = 2(OH_O^{\cdot}) \quad (4)$$

or from the dissociation of water molecules at elevated temperature and the reaction between metal ions and water vapor. These species usually have smaller size and lower charge compared to oxide ion with higher diffusion coefficients, resulting in faster oxidation rate in steam than in oxygen at the same temperature.

Generally, stress generates and accumulates at the oxide scale/substrate interface and within the scale during the oxidation process via different mechanisms. The total stress usually consists of four different sources: thermal stress, growth stress, transformation stress and geometry stress where thermal stress usually contributes to the significant part of total stress [27,33]. The thermal stress coming from the differences in CTEs between the substrate and oxide scale can be estimated by following equation [45],

$$\sigma_{ox} = -\frac{E_{ox}\,(\Delta\alpha)(\Delta T)}{(1-\gamma_{ox})\left[1+\frac{h_{ox}E_{ox}\,(1-\gamma_m)}{h_s\,E_m\,(1-\gamma_{ox})}\right]} \quad (5)$$

the symbols of σ, E, Δα, ΔT, γ, and h correspond to thermal stress, Young's modulus, Poisson's ratio, thermal expansion coefficient difference, temperature difference upon cooling, and thickness, respectively. The subscripts ox and s refer to oxide scale and substrate, respectively. The values of E_{ox} = 400 GPa, E_s = 210 GPa, γ_{ox} = 0.25, γ_s = 0.20, α_{ox} = 8.5× 10^{-6} K^{-1}, α_s = 9.62× 10^{-6} K^{-1} were adopted from references [26,36] to calculate the thermal stress for Ti_2AlC oxidized in steam. The thickness of oxide and substrate were determined from the SEM cross section images. The magnitude of compressive residual stress calculated by Eq. (5) is about 0.86 GPa for Ti_2AlC oxidation at 1400°C in steam for 24 hours, slightly higher than that oxidation at 1400°C in air for 25 hours measured by photostimulated luminescence spectroscopy (0.51 GPa) and that calculated by the same method (0.80 GPa) [26]. The relatively small magnitude of compressive residual stress is attributed to the small difference of CTEs between Al_2O_3 and Ti_2AlC, which is supposed to be insufficient to trigger the fracture or delamination of the oxide scales. Growth stresses, which develop during the isothermal oxidation, can be generated from a number of causes, like volume difference between scale and substrate, compositional or phase changes in the

oxide and substrate, oxide formation within the scale and so on [27]. It is reasonable to surmise that higher levels of growth stresses are produced within the alumina scale when the Ti_2AlC is oxidized in moist atmosphere than that in dry atmosphere. The growth stresses can be generated by the counter diffusion of both anion and cation during oxidation, segregation of titanium oxides at the grain boundaries of α-Al_2O_3 grains and formation of Al_2TiO_5 on the surface with following vaporization of titanium oxides, etc. Once the stress stored in the scale/substrate system exceeds the critical value, it will trigger the stress relaxation process by cracking of the oxide scale and/or by creep of the substrate or oxide. The delamination and fracture, and finally spallation of the oxide scale along with high porosity as shown in Fig.6 (c) and (e) illustrates mechanical disruption of the oxide scale to relief the high stresses, probably mainly growth stresses, built up in the α-Al_2O_3 scale.

Another reasonable explanation for breakaway oxidation at 1400°C in steam is that water vapor decreases the α-Al_2O_3 scale/Ti_2AlC substrate interfacial toughness and α-Al_2O_3 intergranular toughness, which has been widely confirmed for alumina-forming materials [33,46]. Fig.10 shows the SEM images of cross-sectional morphologies of delaminated and compact areas after Ti_2AlC oxidation at 1400°C for 24 hours. Voids were observed at the oxide scale/substrate interface and within the oxide scale. It was argued that the voids were usually generated by the agglomeration of vacancies due to the outward diffusion of cation through the oxide scale or Kirkendall effect [27]. Intragranular and intergranular voids within the Al_2O_3 scale probably first nucleated at the scale/substrate interface prior to being entrapped in the oxide scales. Furthermore, the impurities (Ti_3AlC_2 and free carbon) in the samples probably enhance the development of voids and accelerate the loss of protection effect of the alumina scale as they oxidize much faster. The formation and growth of voids in the scale also has a deleterious effect on the adherence of the oxide scale, causing earlier failure of the scale during oxidation in steam.

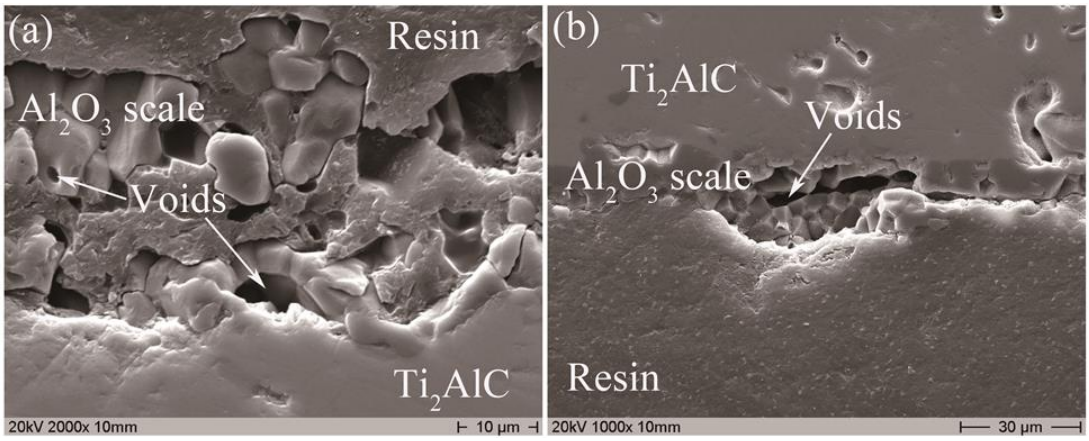

Fig.10 SEM images of typical cross section morphologies of Ti_2AlC oxidation at 1400°C for 24 hours (a) porous area, (b) compact area. Voids were observed at the oxide scale/substrate interface and within the oxide scale.

The development and failure of the oxide scale during Ti_2AlC oxidation at 1400°C in steam is schematically presented in Fig.11. The process can be divided into five main stages as discussed above, i.e. (1) initial oxidation, thin oxide scale roughly corresponds to the composition of the substrate with loose structure, (2) transient oxidation, rapid growth of titanium oxides, leaving Al_2TiO_5 isolated islands on the surface and nucleation of α-Al_2O_3, (3) formation of a continuous α-Al_2O_3 layer and volatile Ti-containing gaseous species with suppressed outward diffusion of Ti and C, simultaneously, nucleation of voids at the oxide scale/substrate interface, (4) thickening and coarsening of α-Al_2O_3 layer with accumulation of stresses, mainly growth stresses, and development of voids, (5) failure of the α-Al_2O_3 layer due to stress relaxation of the scale induced fracture, delamination and cracks.

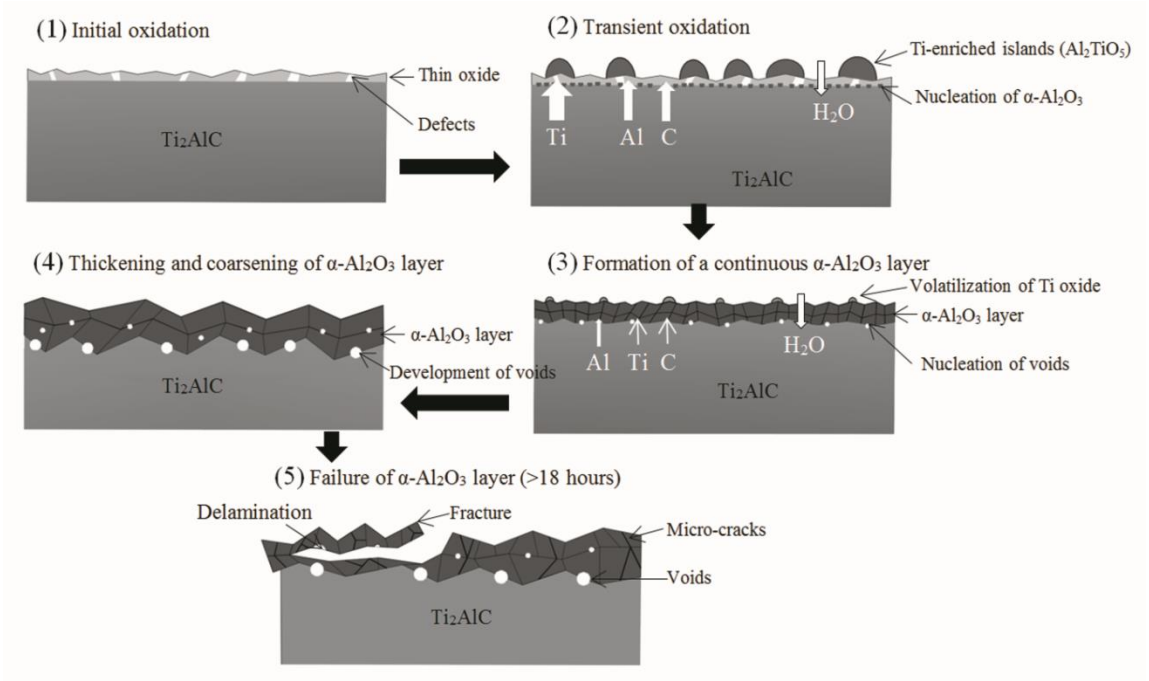

Fig.11 Schematic illustration of growth and failure of the oxide scale on Ti_2AlC during oxidation at 1400°C in steam.

At 1500°C, the α-Al_2O_3 layer cracked already after short oxidation time as shown in Fig.6, which provides short-circuit diffusion pathway for steam and results in loss of protective effect from the early beginning of oxidation. With increasing oxidation temperature, the steam becomes more aggressive and the diffusion rate significantly increases. Hence, the steam can easily penetrate into the matrix during the transient oxidation stage at 1600°C, making the samples rapidly and fully oxidized without formation of alumina scale as demonstrated in the isothermal test at 1600°C.

4. Conclusions

The oxidation behavior of bulk Ti_2AlC MAX phase ceramic in the range of 1400°C - 1600°C in steam for up to 24 hours has been studied. The oxidation kinetics followed a sub-parabolic law at the early stage of oxidation, then transferred to a linear law beyond 18 hours at 1400°C, and obeyed a linear law from the beginning of oxidation at 1500°C. Slightly faster oxidation rate for Ti_2AlC in steam than that in air was attributed to formation of different types of hydrogen-containing species with smaller size and lower charge compared to oxygen. At the early stage of

oxidation below 1600°C, the surface morphologies of Ti_2AlC was rough, consisted of randomly Al_2TiO_5 isolated islands with large elongated grains embedded in a continuous coarse α-Al_2O_3 scale with small irregular grains. The dimensions of Al_2TiO_5 isolated islands gradually decreased with prolonged exposure time and higher temperature due to generation of gaseous Ti-containing species. Even being suppressed, continuous outward diffusion of Ti and C through the α-Al_2O_3 scale still went on after the establishment of a continuous α-Al_2O_3 scale. Titanium oxides segregated at the grain boundaries of α-Al_2O_3 seems acting similar to the "reactive element" during oxidation of FeCrAlRE alloys.

The development and failure of the oxide scale on Ti_2AlC oxidation at 1400°C in steam can be divided into five main stages, i.e. (1) initial oxidation, thin oxide scale roughly corresponds to the composition of the substrate with structural defects, (2) transient oxidation, rapid growth of titanium oxides, leaving Al_2TiO_5 isolated islands on the surface and nucleation of α-Al_2O_3, (3) formation of a continuous α-Al_2O_3 layer and volatile Ti-containing gaseous species with suppressed outward diffusion of Ti and C, simultaneously, nucleation of voids at the oxide scale/substrate interface, (4) thickening and coarsening of α-Al_2O_3 layer with accumulation of stress, growth and development of voids, (5) failure of the α-Al_2O_3 layer due to stress relaxation of the scale induced fracture, delamination and cracks. The scale adhesion in steam is reduced compared to that in air due to the accumulation of high-level stresses, and generation of voids at the scale/substrate interface. The mechanical disruption of the oxide scale contributes to the breakaway oxidation of Ti_2AlC at 1400°C and to the non-protective effect at 1500°C. The impurities (Ti_3AlC_2 and free carbon phases) in the specimens are supposed to accelerate the failure of the protective alumina scale during oxidation. Short-circuit diffusion governs the growth of the α-Al_2O_3 scale with longer oxidation time at 1400°C and from the initial stage of oxidation at 1500°C. The sample was rapidly and completely consumed during isothermal oxidation at 1600°C accompanied by large heat and hydrogen release. The maximum tolerant

temperature of Ti_2AlC in steam was approximate 1555°C determined by a ramp test, which can be extended via a tailored pre-oxidation process.

Acknowledgment

This work was sponsored by the HGF program NUSAFE at Karlsruhe Institute of Technology. C. Tang is grateful for PhD fellowship sponsored by the China Scholarship Council (CSC). The authors would like to thank U. Stegmaier and P. Severloh for support of SEM examinations; Dr. A. Jianu and Dr. A. Weisenburger for providing the Ti_2AlC specimens and Dr. H. Leiste for helpful discussions.

References

[1] B. Cox, Some thoughts on the mechanisms of in-reactor corrosion of zirconium alloys, J. Nucl. Mater. 336 (2005) 331–368. doi:10.1016/j.jnucmat.2004.09.029.

[2] M. Steinbrück, M. Große, L. Sepold, J. Stuckert, Synopsis and outcome of the QUENCH experimental program, Nucl. Eng. Des. 240 (2010) 1714–1727. doi:10.1016/j.nucengdes.2010.03.021.

[3] M. Hirano, T. Yonomoto, M. Ishigaki, N. Watanabe, Y. Maruyama, Y. Sibamoto, et al., Insights from review and analysis of the Fukushima Dai-ichi accident, J. Nucl. Sci. Technol. 49 (2012) 1–17. doi:10.1080/18811248.2011.636538.

[4] S.J. Zinkle, K.A. Terrani, J.C. Gehin, L.J. Ott, L.L. Snead, Accident tolerant fuels for LWRs: A perspective, J. Nucl. Mater. 448 (2014) 374–379. doi:10.1016/j.jnucmat.2013.12.005.

[5] S.M. Bragg-Sitton, Development of advanced accident- tolerant fuels for commercial LWRs, Nucl. News. 53 (2014) 83–91.

[6] C.R.F. Azevedo, Selection of fuel cladding material for nuclear fission reactors, Eng. Fail. Anal. 18 (2011) 1943–1962. doi:10.1016/j.engfailanal.2011.06.010.

[7] M.W. Barsoum, The MN+1AXN phases: a new class of solids; thermodynamically stable nanolaminates, Prog. Solid State Chem. 28 (2000) 201–281. doi:10.1016/S0079-6786(00)00006-6.

[8] Z.M. Sun, Progress in research and development on MAX phases: a family of layered ternary compounds, Int. Mater. Rev. 56 (2011) 143–166. doi:10.1179/1743280410Y.0000000001.

[9] D.J. Tallman, J. Yang, L. Pan, B. Anasori, M.W. Barsoum, Reactivity of Zircaloy-4 with Ti3SiC2 and Ti2AlC in the 1100–1300°C temperature range, J. Nucl. Mater. 460 (2015) 122–129. doi:10.1016/j.jnucmat.2015.02.006.

[10] B.R. Maier, B.L. Garcia-Diaz, B. Hauch, L.C. Olson, R.L. Sindelar, K. Sridharan, Cold spray deposition of Ti2AlC coatings for improved nuclear fuel cladding, J. Nucl. Mater. 466 (2015) 712–717. doi:10.1016/j.jnucmat.2015.06.028.

[11] D.J. Tallman, E.N. Hoffman, E.N. Caspi, B.L. Garcia-diaz, G. Kohse, R.L. Sindelar, et al., Effect of neutron irradiation on select MAX phases, Acta Mater. 85 (2015) 132–143. doi:10.1016/j.actamat.2014.10.068.

[12] D.W. Clark, S.J. Zinkle, M.K. Patel, C.M. Parish, High temperature ion irradiation effects in MAX phase ceramics, Acta Mater. 105 (2016) 130–146. doi:10.1016/j.actamat.2015.11.055.

[13] J. Xiao, T. Yang, C. Wang, J. Xue, Y. Wang, Investigations on Radiation Tolerance of Mn+1AXn Phases: Study of Ti3SiC, Ti3AlC2,Cr2AlC, Cr2GeC, Ti2AlC, and Ti2AlN, J. Am. Ceram. Soc. 98 (2015) 1323–1331. doi:10.1111/jace.13450.

[14] M.W. Barsoum, T. El-Raghy, L.U.J.T. Ogbuji, Oxidation of Ti3SiC2 in air, J. Electrochem. Soc. 144 (1997) 2508–2516. http://www.scopus.com/inward/record.url?eid=2-s2.0-0031190161&partnerID=tZOtx3y1.

[15] Z. Sun, Y. Zhou, High temperature oxidation and hot corrosion behavior of Ti3SiC2-based materials, in: Key Eng. Mater., 2002: pp. 791–796. http://www.scopus.com/inward/record.url?eid=2-s2.0-0036431854&partnerID=tZOtx3y1.

[16] H. Zhang, V. Presser, K.G. Nickel, C. Berthold, Y. Zhou, Hydrothermal Oxidation Behavior of Bulk Titanium Aluminum Carbide, J. Am. Ceram. Soc. 94 (2011) 3460–3466. doi:10.1111/j.1551-2916.2011.04590.x.

[17] S. Basu, N. Obando, A. Gowdy, I. Karaman, M. Radovic, Long-Term Oxidation of Ti2AlC in Air and Water Vapor at 1000–1300°C Temperature Range, J. Electrochem. Soc. 159 (2012) C90. doi:10.1149/2.052202jes.

[18] X.H. Wang, Y.C. Zhou, High-temperature oxidation behavior of Ti2AlC in air, Oxid. Met. 59 (2003) 303–320. doi:10.1023/A:1023092027697.

[19] B. Cui, D.D. Jayaseelan, W.E. Lee, Microstructural evolution during high-temperature oxidation of Ti2AlC ceramics, Acta Mater. 59 (2011) 4116–4125. doi:10.1016/j.actamat.2011.03.035.

[20] Z.J. Lin, M.S. Li, J.Y. Wang, Y.C. Zhou, Influence of water vapor on the oxidation behavior of Ti3AlC2 and Ti2AlC, Scr. Mater. 58 (2008) 29–32. doi:10.1016/j.scriptamat.2007.09.011.

[21] J.L. Smialek, Kinetic Aspects of Ti2AlC MAX Phase Oxidation, Oxid. Met. 83 (2015) 351–366. doi:10.1007/s11085-015-9526-7.

[22] D.J. Tallman, B. Anasori, M.W. Barsoum, A Critical Review of the Oxidation of Ti2AlC, Ti3AlC2 and Cr2AlC in Air, Mater. Res. Lett. 1 (2013) 115–125. doi:10.1080/21663831.2013.806364.

[23] S. Li, G. Song, K. Kwakernaak, S. van der Zwaag, W.G. Sloof, Multiple crack healing of a Ti2AlC ceramic, J. Eur. Ceram. Soc. 32 (2012) 1813–1820. doi:10.1016/j.jeurceramsoc.2012.01.017.

[24] A.-S. Farle, C. Kwakernaak, S. van der Zwaag, W.G. Sloof, A conceptual study into the

potential of Mn+1AXn-phase ceramics for self-healing of crack damage, J. Eur. Ceram. Soc. 35 (2015) 37–45. doi:10.1016/j.jeurceramsoc.2014.08.046.

[25] M. Sundberg, G. Malmqvist, A. Magnusson, T. El-Raghy, Alumina forming high temperature silicides and carbides, Ceram. Int. 30 (2004) 1899–1904. doi:10.1016/j.ceramint.2003.12.046.

[26] J.W. Byeon, J. Liu, M. Hopkins, W. Fischer, N. Garimella, K.B. Park, et al., Microstructure and residual stress of alumina scale formed on Ti 2AlC at high temperature in air, Oxid. Met. 68 (2007) 97–111. doi:10.1007/s11085-007-9063-0.

[27] D.J. Young, High Temperature Oxidation and Corrosion of Metals, Elsevier, 2008. doi:10.1016/S1875-9491(08)00010-0.

[28] H.J. Seifert, A. Kussmaul, F. Aldinger, Phase equilibria and diffusion paths in the Ti-Al-O-N system, J. Alloys Compd. 317–318 (2001) 19–25. doi:10.1016/S0925-8388(00)01409-2.

[29] Z. Lin, M. Zhuo, Y. Zhou, M. Li, J. Wang, Microstructures and adhesion of the oxide scale formed on titanium aluminum carbide substrates, J. Am. Ceram. Soc. 89 (2006) 2964–2966. doi:10.1111/j.1551-2916.2006.01141.x.

[30] J.C. Rao, Y.T. Pei, H.J. Yang, G.M. Song, S.B. Li, J.T.M. De Hosson, TEM study of the initial oxide scales of Ti2AlC, Acta Mater. 59 (2011) 5216–5223. doi:10.1016/j.actamat.2011.04.058.

[31] J. Wang, Y. Zhou, Z. Lin, F. Meng, F. Li, Raman active phonon modes and heat capacities of Ti2AlC and Cr2AlC ceramics: first-principles and experimental investigations, Appl. Phys. Lett. 86 (2005) 101902/1-101902/3. doi:10.1063/1.1873057.

[32] V.T. Witusiewicz, B. Hallstedt, A.A. Bondar, U. Hecht, S.V. Sleptsov, T.Y. Velikanova, Thermodynamic description of the Al–C–Ti system, J. Alloys Compd. 623 (2015) 480–496. doi:10.1016/j.jallcom.2014.10.119.

[33] S.R.J. Saunders, M. Monteiro, F. Rizzo, The oxidation behaviour of metals and alloys at high temperatures in atmospheres containing water vapour: A review, Prog. Mater. Sci. 53 (2008) 775–837. doi:10.1016/j.pmatsci.2007.11.001.

[34] H. Götlind, F. Liu, J.-E. Svensson, M. Halvarsson, L.-G. Johansson, The effect of water vapor on the initial stages of oxidation of the FeCrAl alloy Kanthal AF at 900°C, Oxid. Met. 67 (2007) 251–266. doi:10.1007/s11085-007-9055-0.

[35] M. Barsoum, I. Salama, T. El-Raghy, J. Golczewski, H. Seifert, F. Aldinger, et al., Thermal and electrical properties of Nb2AlC, (Ti, Nb)2AlC and Ti2AlC, Metall. Mater. Trans. A. 33 (2002) 2775–2779. doi:10.1007/s11661-002-0262-7.

[36] X.H. Wang, Y.C. Zhou, Layered Machinable and Electrically Conductive Ti2AlC and Ti3AlC2 Ceramics: A Review, J. Mater. Sci. Technol. 26 (2010) 385–416. doi:10.1016/S1005-0302(10)60064-3.

[37] B.A. Pint, A.J. Garratt-Reed, L.W. Hobbs, The effect of Y and Ti on FeCrAl oxidation at 1400 °C, J. Phys. IV. 3 (1993) 247–255. doi:10.1051/jp4:1993923.

[38] P.Y. Hou, Impurity Effects on Alumina Scale Growth, J. Am. Ceram. Soc. 86 (2003) 660–68. doi:10.1111/j.1151-2916.2003.tb03355.x.

[39] Q.N. Nguyen, High Temperature Volatility and Oxidation Measurements of Titanium and

Silicon Containing Ceramic Materials, Cleveland State University, 2008.

[40] X.H. Wang, Y.C. Zhou, Oxidation behavior of Ti3AlC2 at 1000–1400 °C in air, Corros. Sci. 45 (2003) 891–907. doi:10.1016/S0010-938X(02)00177-4.

[41] M. Magnuson, O. Wilhelmsson, J.-P. Palmquist, U. Jansson, M. Mattesini, S. Li, et al., Electronic structure and chemical bonding in Ti2AlC investigated by soft x-ray emission spectroscopy, Phys. Rev. B. 74 (2006) 1–14. doi:10.1103/PhysRevB.74.205102.

[42] B. Cui, D.D. Jayaseelan, W.E. Lee, TEM study of the early stages of Ti2AlC oxidation at 900°C, Scr. Mater. 67 (2012) 830–833. doi:10.1016/j.scriptamat.2012.07.045.

[43] M.C. Guenette, M.D. Tucker, M. Ionescu, M.M.M. Bilek, D.R. McKenzie, Carbon diffusion in alumina from carbon and Ti2AlC thin films, J. Appl. Phys. 109 (2011) 83503. doi:10.1063/1.3573490.

[44] R.H. Doremus, Diffusion in alumina, J. Appl. Phys. 100 (2006) 101301. doi:10.1063/1.2393012.

[45] J.J. Barnes, J.G. Goedjen, D.A. Shores, A Model for stress generation and relief in Oxide - Metal systems during a temperature change, Oxid. Met. 32 (1989) 449–469. doi:10.1007/BF00665449.

[46] M.C. Maris-side, G.H. Meier, F.S. Pettit, Some Water Vapor Effects during the Oxidation of Alloys that are α -Al2O3 Formers, Metall. Mater. Trans. A. 34A (2003) 2609–2619.

Figure captions

Fig.1 Typical heating and gas flow rate history during isothermal oxidation test in steam.

Fig.2 Oxidation kinetics and surface appearances of Ti_2AlC after oxidation at 1400°C and 1500°C in steam. (a) Mass gain per unit surface area as a function of time with two tests in air. The solid curves indicate fitting relationship between mass gain and oxidation time up to 12 hours. (b) Post-test surface appearances at three different time periods: 1, 12 and 24 hours. The grid in the picture is 5 mm.

Fig.3 Flow rates of H_2, CO, CO_2 per surface area as a function of time for the Ti_2AlC samples oxidized in steam at (a) 1400°C and (b) 1500°C for 18 hours.

Fig.4 X-ray diffraction patterns of oxide scales formed on the surface of Ti_2AlC at (a) 1400°C and (b) 1500°C in steam for six different time periods.

Fig.5 SEM images of typical surface morphologies of Ti_2AlC after oxidation at 1400°C and 1500°C in steam with different time periods and corresponding EDS measurements. See text for detailed description.

Fig.6 SEM images of typical cross section morphologies of Ti_2AlC oxidation at 1400°C and 1500°C in steam with different time periods and the line-scanning profiles along the green line top down in (b) and (f). See text for detailed description.

Fig.7 Flow rates of H_2, CO_2, CO, and CH_4 in the off-gas as a function of time for the Ti_2AlC samples oxidized at 1600°C (a) isothermal test and (b) ramp test. The blue solid line and blue dashed line of the temperature signal represent conditions of pure argon and of a mixture of steam and argon, respectively.

Fig.8 X-ray diffraction patterns of the surface of Ti_2AlC oxidized at 1600°C in steam for the isothermal test (top) and the ramp test (bottom).

Fig.9 SEM images of typical surface morphologies of Ti_2AlC after oxidation at (a) 1400°C for 24 h and (b) 1500°C for 12 h in air.

Fig.10 SEM images of typical cross section morphologies of Ti_2AlC oxidation at 1400°C for 24 hours (a) porous area, (b) compact area. Voids were observed at the oxide scale/substrate interface and within the oxide scale.

Fig.11 Schematic illustration of growth and failure of the oxide scale on Ti_2AlC during oxidation at 1400°C in steam.